Woodhead Publishing Series in Composites Science and Engineering

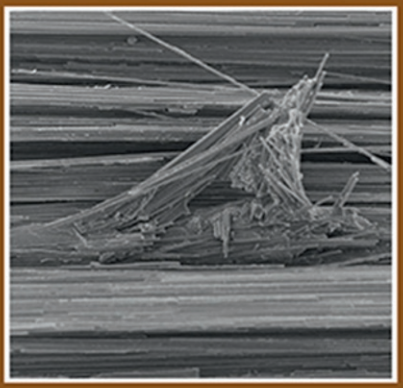

Toughening Mechanisms in Composite Materials

Edited by
Qinghua Qin and
Jianqiao Ye

WP
WOODHEAD PUBLISHING

Toughening Mechanisms in Composite Materials

Related titles

Composite joints and connections
(ISBN 978-1-84569-990-1)

Composite reinforcements for optimum performance
(ISBN 978-1-84569-965-9)

Non-crimp fabric composites
(ISBN 978-1-84569-762-4)

Woodhead Publishing Series in Composites Science and Engineering: Number 55

Toughening Mechanisms in Composite Materials

Edited by

Qinghua Qin and Jianqiao Ye

AMSTERDAM • BOSTON • CAMBRIDGE • HEIDELBERG
LONDON • NEW YORK • OXFORD • PARIS • SAN DIEGO
SAN FRANCISCO • SINGAPORE • SYDNEY • TOKYO
Woodhead Publishing is an imprint of Elsevier

Woodhead Publishing is an imprint of Elsevier
80 High Street, Sawston, Cambridge, CB22 3HJ, UK
225 Wyman Street, Waltham, MA 02451, USA
Langford Lane, Kidlington, OX5 1GB, UK

Copyright © 2015 Elsevier Ltd. All rights reserved

No part of this publication may be reproduced, stored in a retrieval system or transmitted in any form or by any means electronic, mechanical, photocopying, recording or otherwise without the prior written permission of the publisher.

Permissions may be sought directly from Elsevier's Science & Technology Rights Department in Oxford, UK: phone (+44) (0) 1865 843830; fax (+44) (0) 1865 853333; email: permissions@elsevier.com. Alternatively you can submit your request online by visiting the Elsevier website at http://elsevier.com/locate/permissions, and selecting Obtaining permission to use Elsevier material.

Notice
No responsibility is assumed by the publisher for any injury and/or damage to persons or property as a matter of products liability, negligence or otherwise, or from any use or operation of any methods, products, instructions or ideas contained in the material herein. Because of rapid advances in the medical sciences, in particular, independent verification of diagnoses and drug dosages should be made.

British Library Cataloguing in Publication Data
A catalogue record for this book is available from the British Library.

Library of Congress Control Number: 2015931787

ISBN 978-1-78242-279-2 (print)
ISBN 978-1-78242-291-4 (online)

For information on all Woodhead Publishing publications visit our website at http://store.elsevier.com/

Contents

List of contributors

G. Allegri Imperial College London, London, UK

S. Araby School of Engineering, University of South Australia (UniSA), Salisbury, SA, Australia

C. B. Emrullahoglu Abi Afyon Kocatepe University, Afyonkarahisar, Turkey

K. Bilge Sabanci University, Istanbul, Turkey

M. Esmkhani Iran University of Science and Technology, Tehran, Iran

S.M. Ghoreishi Iran University of Science and Technology, Tehran, Iran

M. Kašiarová Slovak Academy of Sciences, Košice, Slovak Republic

V. Kompiš University of Žilina, Žilina, Slovakia

T. Kusaka Ritsumeikan University, Kusatsu, Japan

J.K. Lander Rolls-Royce Plc, Derby, UK

X. Lin University of New South Wales, Canberra, ACT, Australia

X. Liu Beijing University of Technology, Beijing, China

J. Ma School of Engineering, University of South Australia (UniSA), Salisbury, SA, Australia

Q. Meng School of Engineering, University of South Australia (UniSA), Salisbury, SA, Australia

Z. Mouti Eaton, West Midlands, UK

Z. Murčinková Technical University, Košice, Slovakia

J. Njuguna Robert Gordon University, Aberdeen, UK

M. Papila Sabanci University, Istanbul, Turkey

I.K. Partridge University of Bristol, Bristol, UK

Q.H. Qin Australian National University, Acton, ACT, Australia

M. Quaresimin University of Padova, Vicenza, Italy

M. Salviato University of Padova, Vicenza, Italy, and Northwestern University, Evanston, IL, USA

M.M. Shokrieh Iran University of Science and Technology, Tehran, Iran

P. Tatarko Slovak Academy of Sciences, Košice, Slovak Republic, and Queen Mary University of London, London, UK

H. Tian The University of New South Wales, Canberra, ACT, Australia

K. Westwood Eaton, West Midlands, UK

Q.-S. Yang Beijing University of Technology, Beijing, China

M. Yasaee University of Bristol, Bristol, UK

M. Zappalorto University of Padova, Vicenza, Italy

Y.X. Zhang The University of New South Wales, Canberra, ACT, Australia

M. Žmindák University of Žilina, Žilina, Slovakia

Woodhead Publishing Series in Composites Science and Engineering

1 **Thermoplastic aromatic polymer composites**
F. N. Cogswell
2 **Design and manufacture of composite structures**
G. C. Eckold
3 **Handbook of polymer composites for engineers**
Edited by L. C. Hollaway
4 **Optimisation of composite structures design**
A. Miravete
5 **Short-fibre polymer composites**
Edited by S. K. De and J. R. White
6 **Flow-induced alignment in composite materials**
Edited by T. D. Papthanasiou and D. C. Guell
7 **Thermoset resins for composites**
Compiled by Technolex
8 **Microstructural characterisation of fibre-reinforced composites**
Edited by J. Summerscales
9 **Composite materials**
F. L. Matthews and R. D. Rawlings
10 **3-D textile reinforcements in composite materials**
Edited by A. Miravete
11 **Pultrusion for engineers**
Edited by T. Starr
12 **Impact behaviour of fibre-reinforced composite materials and structures**
Edited by S. R. Reid and G. Zhou
13 **Finite element modelling of composite materials and structures**
F. L. Matthews, G. A. O. Davies, D. Hitchings and C. Soutis
14 **Mechanical testing of advanced fibre composites**
Edited by G. M. Hodgkinson
15 **Integrated design and manufacture using fibre-reinforced polymeric composites**
Edited by M. J. Owen and I. A. Jones
16 **Fatigue in composites**
Edited by B. Harris
17 **Green composites**
Edited by C. Baillie

18 **Multi-scale modelling of composite material systems**
Edited by C. Soutis and P. W. R. Beaumont
19 **Lightweight ballistic composites**
Edited by A. Bhatnagar
20 **Polymer nanocomposites**
Y-W. Mai and Z-Z. Yu
21 **Properties and performance of natural-fibre composite**
Edited by K. Pickering
22 **Ageing of composites**
Edited by R. Martin
23 **Tribology of natural fiber polymer composites**
N. Chand and M. Fahim
24 **Wood-polymer composites**
Edited by K. O. Niska and M. Sain
25 **Delamination behaviour of composites**
Edited by S. Sridharan
26 **Science and engineering of short fibre reinforced polymer composites**
S-Y. Fu, B. Lauke and Y-M. Mai
27 **Failure analysis and fractography of polymer composites**
E. S. Greenhalgh
28 **Management, recycling and reuse of waste composites**
Edited by V. Goodship
29 **Materials, design and manufacturing for lightweight vehicles**
Edited by P. K. Mallick
30 **Fatigue life prediction of composites and composite structures**
Edited by A. P. Vassilopoulos
31 **Physical properties and applications of polymer nanocomposites**
Edited by S. C. Tjong and Y-W. Mai
32 **Creep and fatigue in polymer matrix composites**
Edited by R. M. Guedes
33 **Interface engineering of natural fibre composites for maximum performance**
Edited by N. E. Zafeiropoulos
34 **Polymer-carbon nanotube composites**
Edited by T. McNally and P. Pötschke
35 **Non-crimp fabric composites: Manufacturing, properties and applications**
Edited by S. V. Lomov
36 **Composite reinforcements for optimum performance**
Edited by P. Boisse
37 **Polymer matrix composites and technology**
R. Wang, S. Zeng and Y. Zeng
38 **Composite joints and connections**
Edited by P. Camanho and L. Tong
39 **Machining technology for composite materials**
Edited by H. Hocheng
40 **Failure mechanisms in polymer matrix composites**
Edited by P. Robinson, E. S. Greenhalgh and S. Pinho
41 **Advances in polymer nanocomposites: Types and applications**
Edited by F. Gao

42 **Manufacturing techniques for polymer matrix composites (PMCs)**
Edited by S. Advani and K-T. Hsiao
43 **Non-destructive evaluation (NDE) of polymer matrix composites: Techniques and applications**
Edited by V. M. Karbhari
44 **Environmentally friendly polymer nanocomposites: Types, processing and properties**
S. S. Ray
45 **Advances in ceramic matrix composites**
Edited by I. M. Low
46 **Ceramic nanocomposites**
Edited by R. Banerjee and I. Manna
47 **Natural fibre composites: Materials, processes and properties**
Edited by A. Hodzic and R. Shanks
48 **Residual stresses in composite materials**
Edited by M. Shokrieh
49 **Health and environmental safety of nanomaterials: Polymer nanocomposites and other materials containing nanoparticles**
Edited by J. Njuguna, K. Pielichowski and H. Zhu
50 **Polymer composites in the aerospace industry**
Edited by P. E. Irving and C. Soutis
51 **Biofiber reinforcement in composite materials**
Edited by O. Faruk and M. Sain
52 **Fatigue and fracture of adhesively-bonded composite joints: Behaviour, simulation and modelling**
Edited by A. P. Vassilopoulos
53 **Fatigue of Textile Composites**
Edited by V. Carvelli and S. V. Lomov
54 **Wood Composites – From Nanocellulose to Superstructures**
Edited by M. Ansell
55 **Toughening Mechanisms in Composite Materials**
Edited by Q. Qin and J. Ye

This page intentionally left blank

Introduction to the composite and its toughening mechanisms

1

Q.H. Qin
Australian National University, Acton, ACT, Australia

1.1 Basic concepts

The word "composite" usually signifies that two or more separate materials are combined on a macroscopic scale to form a structural unit for various engineering applications. Each of the material components may have distinct thermal, mechanical, electrical, magnetic, optical, and chemical properties. It is noted that a composite composed of an assemblage of these different materials gives us a useful new material whose performance characteristics are superior to those of the constituent materials acting independently (Ye, 2003; Qin and Yang, 2008). One or more of the material components is usually discontinuous, stiffer, and stronger and known as the reinforcement; the less stiff and weaker material is continuous and called the matrix. Sometimes, because of chemical interactions or other processing effects, an additional distinct phase, called an interphase, exists between the reinforcement and the matrix (Damiel and Ishai, 2006). Composite materials have some advantages when compared to their components or metal parts. Some material properties that can be improved by forming a composite material are (Jones, 1999):

- Strength
- Stiffness
- Wear resistance
- Weight
- Fatigue life
- Extreme temperature response
- Thermal insulation or conduction
- Electrical insulation or conduction
- Acoustical insulation or conduction
- Response to nuclear, X-ray, or magnetic radiation
- Chemical response or inertness to an environment (corrosion resistance)
- Electromagnetic and radar insulation or conduction
- Crack (fracture) resistance and arrest
- Cost
- Fabrication
- Temperature-dependent behavior
- Attractiveness.

Further, composite materials have the following advantages: (1) composites can have unique properties (e.g., specific strength and modulus) that are significantly better

Toughening Mechanisms in Composite Materials. http://dx.doi.org/10.1016/B978-1-78242-279-2.00001-9
Copyright © 2015 Elsevier Ltd. All rights reserved.

than their metal, polymer, and ceramic counterparts; (2) composites offer a greater flexiblity in designing and manufacturing a specific engineering structure; (3) composites can be fabricated to a final product from raw materials; and (4) composites can be tailored to have given properties required by the end users.

1.1.1 Matrix materials

Polymers, metals, and ceramics are all used as matrix materials in composites. They are the constituents that are continuously distributed in a composite. Examples of matrix materials are (1) polymers: epoxies, polyesters, phenolics, silicone, polyimide, nylon, polyethelene, polystyrene, and polycarbonate. The first five belong to the category of thermoset plastic, which is the material that can be melted and shaped only once (if it is heated a second time, it tends to crack or disintegrate); whereas the last four are categorized as thermoplastic, which is, in contrast, a material that can be melted and shaped over and over again; (2) metals: steel, iron, aluminum, zinc, carbon, copper, nickel, silver, titanium, and magnesium; and (3) ceramics: alumina, silicon carbide, aluminum nitride, silicon nitride, zirconia, and mullite. The functions of the matrix are to transmit forces between fibers, hold fibers in proper orientations, protect fibers from the environment, and stop cracks from spreading between fibers. To effectively realize those functions, a desired matrix material should have good ductility, high toughness and interlaminar shear strength, stable temperature properties, and high moisture/environmental resistance. In addition, a strong interface bond between the fiber and matrix materials is desirable, so the matrix must be capable of developing a mechanical or chemical bond with the fiber (Gibson, 2012).

1.1.2 Reinforcement materials

Reinforcement materials usually add rigidity and greatly impede crack propagation. In particular, they enforce the mechanical properties of the matrix and, in most cases, are harder, stronger, and stiffer than the matrix. The reinforcement can be divided into four basic categories: fibers, particulates, fillers, and flakes.

Flakes are in flat platelet form and have a primarily two-dimensional geometry with strength and stiffness in two directions. They can form an effective composite material when suspended in a glass or plastic. Ordinarily, flakes are packed parallel to one another with a resulting higher density than fiber-packing concepts. Typical flake materials are mica, aluminum, and silver. Mica flakes embedded in a glassy matrix provide composites that can be machined easily and are used in electrical applications. Aluminum flakes are commonly used in paints and other coatings in which they orient themselves parallel to the surface of the coating. Silver flakes are used where good conductivity is required.

Fillers are particles or powders added to material to change and improve the physical and mechanical properties of composites. They are also used to lower the consumption of a more expensive binder material. In particular, fillers are used to modify or enhance properties such as thermal conductivity, electrical resistivity, friction, wear resistance, and flame resistance. Typical fillers are calcium carbonate,

aluminum oxide, lime (also known as calcium oxide), fumed silica, treated clays, and hollow glass beads.

Particulates used in composites can be small particles (<0.25 μm), hollow spheres, cubes, platelets, or carbon nanotubes. In each case, the particulates provide desirable material properties, and the matrix acts as a binding medium necessary for structural applications. The arrangement of particulate materials may be random or with a preferred orientation. In general, particles are not very effective in improving strength and fracture resistance. Typical particle materials are lead, copper, tungsten, molybdenum, and chromium.

Finally, a fiber is a rope or string used as a component of composite materials whose aspect ratio (length/diameter) is usually very large (>100). The cross-section can be circular, square, or hexagonal. Commonly used fibers in the composite include the following: (1) glass fiber, which consists primarily of silicon dioxide and metallic oxide modifying elements and are generally produced by mechanical drawing of molten glass through a small orifice. They are widely used due to low cost and high corrosion resistance. Glass fibers can be used in fishing rods, storage tanks, and aircraft parts; (2) aramid fiber, which has higher specific strength and is lighter than glass, is more ductile than carbon. Examples of industrial application are armor, protective clothing, and sporting goods; (3) carbon fiber, which is often produced from an oxidized polyacrylonitrile or via pyrolysis carbonized polymers. The carbon fiber can have a modulus as high as 950 GPa with low density. Its diameter is usually between 5 and 8 μm, smaller than a human hair (50 μm); (4) boron fiber, which usually has high stiffness, good compressive strength, and large diameters (0.05–0.2 mm) compared to other types of fibers. Composites with boron fibers are widely used in aerospace structures where high stiffness is needed; and (5) silicon carbide fiber, which is usually used in high-temperature metal and ceramic matrix composites (CMC) because of its excellent oxidation resistance, high modulus, and strength in high-temperature atmosphere.

1.2 Historical developments

Although it is difficult to say when or where people first learned about composites, nature and literature provide us with numerous examples. About 3000 BC, people used brick made of straw and mud for construction. Mud reinforced with bamboo shoots and glued laminated wood were used in houses built by the Egyptians in 1500 BC. Mongols invented the first composite bow in 1200 AD. Glass–polyester radomes were introduced in 1938 for application in aerospace structures: here, the fiberglass was combined for the first time with good unsaturated polyester resins. The first molded fiberglass boat was built in 1942. The U.S. government patented the first filament winding process in 1946, followed by missile applications in the 1950s. In 1952, Herring and Galt (1952) described the mechanical properties of thin whiskers of Sn, and inferred that whiskers were single crystals. Boeing 727 started to employ reinforced plastic components in 1960. The first boron and high-strength

carbon fibers were introduced in the early 1960s. It was not until 1969 that carbon/epoxy materials were applied to operational fighter aircraft structures. Metal matrix composites (MMC) such as boron/aluminum were introduced in 1970. DuPont developed Kevlar fibers in early 1970s (Greenwoo and Rose, 1974). Starting in the late 1970s, the application of composites has greatly increased and expended to tennis rackets, large-diameter thin-walled pipes, civilian structural members, golf clubs, automobile and truck components, skis, fiber-reinforced concrete, epoxy-impregnated concrete, composite-pressure vessels, armor, space vehicles, boats, and airplanes, due to the development of new fibers such as carbon, boron, and nanotube and new composite systems with matrix made of polymers and metals.

1.3 Classification and applications

There are two classification systems of composite materials. One is based on the type of matrix material (metal, ceramic, polymer, carbon/graphite) and the second is based on the geometry of reinforcing material (fiber, whisker, flake, and particulate).

1.3.1 Classification based on matrix materials

Based on matrix materials, four commonly accepted composites are:

- MMC are composite materials with at least two constituent parts, one being a metal (aluminum, magnesium, iron, cobalt, copper), which is considered as the matrix phase. The other material may be a different metal (lead, tungsten, molybdenum) or another material (oxides, carbides, organic compound). Typical engineering structures containing MMC include carbide drills, tank armor, automotive disc brakes, automotive engines, and the F-16 Fighting Falcon.
- CMC are composed of a ceramic matrix and embedded fibers of other ceramic material (dispersed phase). Advantages of CMC include high strength and hardness at very high temperature, high service temperature limits for ceramics, low density, and chemical inertness. The applications of CMCs are in fields requiring reliability at high temperatures (beyond the capability of metals) and resistance to corrosion and wear (e.g., heat shield systems for space vehicles; components for high-temperature gas turbines; components for burners, flame holders, and hot gas ducts; and components for slide bearings under heavy loads requiring high corrosion and wear resistance).
- Polymer matrix composites (PMC) are composed of a matrix from thermoset (epoxies, phenolics) or thermoplastic (polycarbonate, polyvinylchloride, nylon, acrylics) and embedded glass, carbon, steel, or Kevlar fibers. Unlike a CMC, in which the reinforcement is used primarily to improve the fracture toughness, the reinforcement in a PMC provides high strength and stiffness. The advantages of PMC are attributed to its light weight, high stiffness and strength along the direction of the reinforcement, and superior corrosion and fatigue resistance compared to metals. Examples of PMC application are secondary load-bearing aerospace structures, boat bodies, canoes, kayaks, automotive parts, radio-controlled vehicles,

sporting goods (golf clubs, skis, tennis racquets, fishing rods), bullet-proof vests and other armor parts, and brake and clutch linings.

- Carbon–carbon composites (C/C) consist of carbon fibers embedded in a carbonaceous matrix. Carbon is a very versatile material that can exist in a variety of forms: amorphous, graphite, diamond, pyrolytic graphite, carbon black, carbon nanotube, fullerenes, and grapheme. Carbon is an excellent high-temperature material used in an inert or nonoxidizing atmosphere. The working temperature can be as high as 2000 °C. Typical high-temperature applications involve breaks for aircraft and automobiles, dies for use in hot-pressing, high-temperature fasteners, heating elements in furnaces and protection tubes, and space shuttle nose cones.

1.3.2 Classification based on the geometry of reinforcement

There are four typical types of composites based on the geometry of reinforcement:

- Fiber-reinforced composites (FRC) consist of three components: (1) the fibers as the discontinuous or dispersed phase; (2) the matrix as the continuous phase; and (3) the fine interphase region, also known as the interface. The fiber may be of short (discontinuous) or long (continuous) fiber. As indicated in Gibson (2012), in a fiber composite, commonly used matrix materials are epoxy, aluminum, calcium-alumino silicate, polymer, and carbon. Examples of FRP application are bridges and columns, prestressing tendons, reinforcing bars, grid reinforcement, and dowels. In addition, FRC is also used in outdoor deck floors, railings, fences, cladding and siding, park benches, and window and door frames.
- Whisker composites are composed of a matrix material and embedded reinforcing whisker materials (e.g., potassium titanate whisker, graphite, aluminum oxide, silicon carbide, silicon oxide, boron carbide, and beryllium oxide). A whisker is the nearly perfect, single-crystal material produced synthetically under controlled conditions. It is a very thin, short filament with large length/diameter ratio and is smaller than chopped fibers. Owing to its small diameter, the whisker is nearly free of internal defects and yields strength close to the maximum theoretical value. For example, whiskers of silicon nitride are being made as fine as 0.2–0.5 μm in diameter. Tjong and Meng (1999) found that whiskers could have much higher specific strength than short glass or carbon fibers and could reinforce polymers more effectively.
- Flake composites consist of flat reinforcements of matrices. Typical flake materials are glass, mica, aluminum, and silver. As indicated in Kaw (2006), flake composites provide advantages such as high out-of-plane flexural modulus, high strength, and low cost. However, flakes cannot be oriented easily and only a limited number of materials are available for use.
- Particulate composites consist of particles of various sizes and shapes randomly dispersed within the matrix. Because of the usual randomness of particle distribution, these composites can be regarded as quasi-homogeneous and quasi-isotropic on a scale much larger than the particle size and spacing. Particulate composites have advantages such as improved strength, increased operating temperature, oxidation resistance, high creep resistance, and high strength to weight ratio (Kaw, 2006). Typical examples of application are appliances, toys, cell phone casings, helmets, body panels of automotive cars, breaks, bumpers, and intake manifolds.

1.4 Effective mechanical behavior of composites

As indicated in Section 1.1, a composite is composed of two or more separate materials. Each of the material components may have distinct material properties. It is important to determine the effective material properties if we replace the composite with a homogeneous material. In classical mechanics, at a macrolevel, the material properties are always assumed to be homogeneous on an average basis, whereas at a microlevel, i.e., inside the composite, the material properties are heterogeneous. At a microlevel, the heterogeneous microstructure and physical laws are usually known. The task is to find homogeneous material properties at a macrolevel based on the information of microstructure. These properties are often called overall material properties or effective material properties, and the process is often known as homogenization. Recently, some investigations have been made into the composite array using methods such as the homogenization method (Qin and Yang, 2008). Grassi et al. (2002) numerically examined the effect of fiber volume fraction of the through thickness Young's modulus. Qin (2004a,b, 2005) and Yang and Qin (2004) presented several boundary elements–micromechanics models for predicting effective properties of materials with defects or inclusions. Antoniou et al. (2009) developed a FE model to predict mechanical behavior of glass/epoxy tubes under static loading. Xu et al. (2008) conducted an experiment on the plate size in determining the effective modulus. Yang and Qin (2001, 2003) used the finite element method (FEM) to predict effective elasto-plastic properties of composites. To determine the ranges of effective properties using various micromechanics models, the Voigt and Reuss rule (Gasik, 1998) presented a method to find the upper and lower bounds, respectively, of the stiffness for a composite material with arbitrary fiber-matrix geometry. Micromechanic models were also used to determine effective properties of piezoelectric materials with cracks (Qin et al., 1998; Yu and Qin, 1996; Qin and Yu, 1997), microvoids (Qin and Yu, 1998), and of human dentine materials (Wang and Qin, 2007, 2011; Qin and Swain, 2004). Several other research studies have used representative unit cell models to investigate the dependence of component properties on composite materials (Tvergaard, 1990; Bao et al., 1991; Zahl and McMeeking, 1991; Levy and Papazian, 1990; Li et al., 1995; Feng et al., 2003). This section briefly describes major micromechanics models commonly used to determine effective material properties and to analyze the corresponding mechanical behavior of composite materials. It includes the mechanics of materials approach (MMA), finite element modeling, direct and indirect homogenization, and boundary element approach.

1.4.1 Mechanics of materials approach

MMA provides an analytical technique to calculate effective material properties of the fiber-reinforced composites. These overall material properties can be used to predict the material behavior with various interfaces. MMA is used to determine the overall material properties due to their respective fiber and matrix volume fractions and constituent material properties. It assumes an average of stresses and strains to examine the global response.

1.4.1.1 Determination of longitudinal modulus E_1

We begin with determining the Young's modulus E_1 (Young's modulus in the fiber direction) of a fiber-reinforced composite. To this end, consider a representative volume element (RVE) in Figure 1.1. It is subjected to a longitudinal normal stress σ_1, as shown in Figure 1.1. Static equilibrium requires that the total resultant force F on the RVE must equal the sum of the forces acting on the fiber and matrix:

$$F = \sigma_1 A = \overline{\sigma}_{m1} A_m + \overline{\sigma}_{f1} A_f \tag{1.1}$$

where subscripts "m" and "f" refer to matrix and fiber, A, A_m, and A_f stand for cross areas of composite, matrix, and fiber respectively, and

$$\overline{\sigma}_{m1} = \frac{1}{V}\int \sigma_{m1} dV = \frac{1}{A}\int \sigma_{m1} dA, \quad \overline{\sigma}_{f1} = \frac{1}{V}\int \sigma_{f1} dV = \frac{1}{A}\int \sigma_{f1} dA \tag{1.2}$$

Since the length of matrix and fiber are the same (Figure 1.1), area fractions are equal to the corresponding volume fractions. As such, Eq. (1.1) can be rearranged to give a "rule of mixtures" for longitudinal stress:

$$\sigma_1 = \overline{\sigma}_{m1}\frac{A_m}{A} + \overline{\sigma}_{f1}\frac{A_f}{A} = \overline{\sigma}_{m1} v_m + \overline{\sigma}_{f1} v_f \tag{1.3}$$

where v_m and v_f are area fraction of matrix and fiber, respectively.

If both the matrix and fiber are linear elastic and isotropic, we have from Hooke's law

$$\sigma_1 = E_1 \overline{\varepsilon}_1, \quad \sigma_{m1} = E_m \overline{\varepsilon}_{m1}, \quad \sigma_{f1} = E_f \overline{\varepsilon}_{f1} \tag{1.4}$$

where

$$\overline{\varepsilon}_1 = \frac{1}{A}\int \varepsilon_1 dA, \quad \overline{\varepsilon}_{m1} = \frac{1}{A}\int \varepsilon_{m1} dA, \quad \overline{\sigma}_{f1} = \frac{1}{A}\int \varepsilon_{f1} dA \tag{1.5}$$

and Eq. (1.3) becomes

$$E_1 \overline{\varepsilon}_1 = E_m \overline{\varepsilon}_m v_m + E_f \overline{\varepsilon}_f v_f \tag{1.6}$$

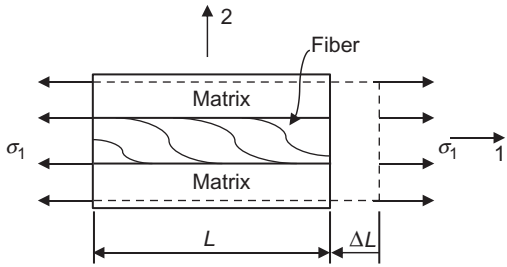

Figure 1.1 Composite loaded in fiber direction.

If the matrix and fiber are perfectly bonded, the average strains in the composite, matrix, and fiber along the one direction are all equal:

$$\overline{\varepsilon}_1 = \overline{\varepsilon}_{m1} = \overline{\varepsilon}_{f1} \tag{1.7}$$

Combination of Eqs. (1.6) and (1.7) yields the rule of mixtures for the longitudinal modulus:

$$E_1 = E_f v_f + E_m v_m \tag{1.8}$$

1.4.1.2 Determination of transverse modulus E_2

The Young's modulus of the composite material in the transverse direction can be determined by considering the loading case shown in Figure 1.2.

With the loading case in Figure 1.2, the normal strains in the fiber and matrix are found to be

$$\varepsilon_{f2} = \frac{\sigma_2}{E_f}, \quad \varepsilon_{m2} = \frac{\sigma_2}{E_m} \tag{1.9}$$

The total elongation in the transverse direction is $\Delta W = \varepsilon_2 W$ on average. It should be equal to the sum of the corresponding transverse elongation in the fiber, $W_f \varepsilon_{f2}$, and the matrix, $W_m \varepsilon_{m2}$:

$$\Delta W = \varepsilon_2 W = \frac{W}{E_2}\sigma_2 = \varepsilon_{f2} W_f + \varepsilon_{m2} W_m = \left(\frac{W_f}{E_f} + \frac{W_m}{E_m}\right)\sigma_2 \tag{1.10}$$

where W, W_f, and W_m are, respectively, the width of composite, fiber, and matrix. Equation (1.10) can be reduced to the "inverse rule of mixtures" for E_2 by dividing W on both sides of the equation:

$$\frac{1}{E_2} = \frac{v_f}{E_f} + \frac{v_m}{E_m} \tag{1.11}$$

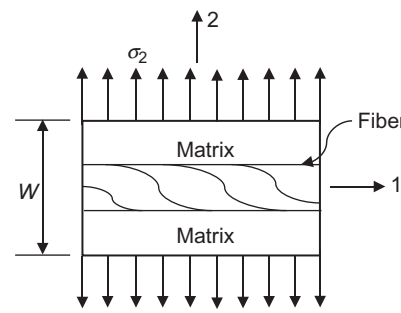

Figure 1.2 Composite loaded in transverse direction.

1.4.1.3 Determination of major Poisson's ratio μ_{12}

The major Poisson's ratio μ_{12}, is obtained by an approach similar to the derivation for E_1. For the loading case shown in Figure 1.1, the major Poisson's ratio is defined as:

$$\mu_{12} = -\frac{\varepsilon_2}{\varepsilon_1} \tag{1.12}$$

The transverse deformation ΔW is then equal to $\varepsilon_2 W = -W\mu_{12}\varepsilon_1$. In a manner of the derivation for E_2, the transverse deformation in the fiber, ΔW_f, and the matrix, ΔW_m, are given as

$$\Delta W_m = W v_m \mu_m \varepsilon_1, \quad \Delta W_f = W v_f \mu_f \varepsilon_1 \tag{1.13}$$

Since geometric compatibility requires that $\Delta W = \Delta W_f + \Delta W_m$, we have

$$\mu_{12} = \mu_m v_m + \mu_f v_f \tag{1.14}$$

This gives the rule of mixtures for the major Poisson's ratio.

1.4.1.4 Determination of in-plane shear modulus G_{12}

Consider the loading case shown in Figure 1.3a. The in-plane shear modulus of a lamina, G_{12}, is determined in the mechanics of materials method by assuming that the shearing stresses on the fiber and on the matrix are the same. From this assumption, we obtain:

$$\gamma = \frac{\tau}{G_{12}}, \quad \gamma_m = \frac{\tau}{G_m}, \quad \gamma_f = \frac{\tau}{G_f} \tag{1.15}$$

The shear deformations in matrix and fiber are then given as (Figure 1.3b):

$$\Delta_m = \gamma_m W_m = \gamma_m v_m W, \quad \Delta_f = \gamma_f W_f = \gamma_f v_f W \tag{1.16}$$

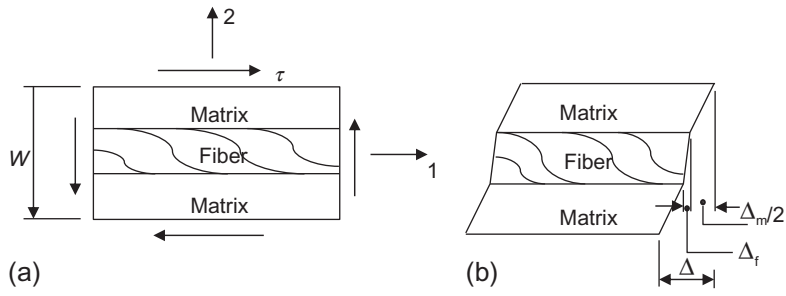

Figure 1.3 Composite loaded with shear stress.

The total shear deformation is $\Delta = \gamma W$, which is made up of approximate microscopic deformations (Figure 1.3). Again, geometric compatibility requires that $\Delta = \Delta_f + \Delta_m$ (Figure 1.3b), which yields by dividing W:

$$\gamma = \gamma_m v_m + \gamma_f v_f \tag{1.17}$$

Substituting Eq. (1.15) into Eq. (1.17), we have

$$\frac{1}{G_{12}} = \frac{v_m}{G_m} + \frac{v_f}{G_f} \tag{1.18}$$

1.4.2 Finite element approach

In order to obtain values for the material properties of fiber-reinforced composites using an FEM, the basic formulations are briefly described in this section. These differ to MMA in that they relate to the basic understanding of stress/strain relations and are not directly related to the volume fractions as stated in Section 1.4.1.

1.4.2.1 Calculation of E_1 and μ_{12}

E_1 and μ_{12} can be determined by considering the loading case shown in Figure 1.1, where a stress σ_1 is applied in the fiber direction of the composite. The effective Young's modulus and major Poisson ratio are, then, evaluated by

$$E_1 = \frac{\overline{\sigma}_1}{\overline{\varepsilon}_1} = \frac{\int_V \sigma_1 \, dV/V}{\int_V \varepsilon_1 \, dV/V} = \frac{\int_V \sigma_1 \, dV}{\int_V \varepsilon_1 \, dV}, \quad v_{12} = -\frac{\overline{\varepsilon}_2}{\overline{\varepsilon}_1} = -\frac{\int_V \varepsilon_2 \, dV/V}{\int_V \varepsilon_1 \, dV/V} = -\frac{\int_V \varepsilon_2 \, dV}{\int_V \varepsilon_1 \, dV} \tag{1.19}$$

If the left end is fixed and $\Delta\overline{L}$ represents the average displacement at the right end, the average strain can be defined as

$$\overline{\varepsilon} = \frac{\Delta\overline{L}}{L} \tag{1.20}$$

Therefore, the major task for FE calculation is to determine $\Delta\overline{L}$ and the average stress $\overline{\sigma}_1$. Further, the calculation of major Poisson ratio requires the information of $\varepsilon_2 = \Delta W/W$. As a result, the major issue for FE calculation is to calculate average transverse displacement ΔW. This has been implemented into our FE program.

1.4.2.2 Calculation of E_2

Considering the loading case as shown in Figure 1.2, the effective transverse Young's modulus E_2 is defined as

$$E_2 = \frac{\overline{\sigma}_2}{\overline{\varepsilon}_2} = \frac{\int_V \sigma_2 \mathrm{d}V/V}{\int_V \varepsilon_2 \mathrm{d}V/V} = \frac{\int_V \sigma_2 \mathrm{d}V}{\int_V \varepsilon_2 \mathrm{d}V} \tag{1.21}$$

where $\overline{\varepsilon}_2 = \Delta\overline{W}/W$. The major task for FE calculation is, then, to determine $\Delta\overline{W}$ and the average stress $\overline{\sigma}_2$.

1.4.2.3 Calculation of G_{12}

The in-plane shear modulus of a fiber-reinforced composite can be determined by considering the loading case shown in Figure 1.3, a shear stress is applied over the boundary of the composite.

$$G_{12} = \frac{\overline{\tau}}{\overline{\gamma}} = \frac{\int_V \tau \mathrm{d}V/V}{\int_V \gamma \mathrm{d}V/V} = \frac{\int_V \tau \mathrm{d}V}{\int_V \gamma \mathrm{d}V} \tag{1.22}$$

Considering the fact that the shear strain can be defined as u/y, where u is displacement in fiber direction and y stands for the vertical coordinate originated at the bottom of the composite, the task of FE calculation, in this case, is to evaluate shear stress and the displacement u.

From these equations, we can determine E_1, E_2, and G_{12}, noting that all other stresses and strains are taken as zero except for the stress and strain along the direction for the material property being determined.

1.4.2.4 A numerical example

As a numerical illustration, consider a composite composted of carbon fiber and epoxy resin matrix. Table 1.1 lists the mechanical properties of materials used in finite element approach (FEA).

To study effects of fiber's geometry on the overall properties of the composite, the following six combinations of geometry are considered: (a) rectangular matrix with circular fibers (RMCF); (b) rectangular matrix with hexagonal fibers (RMHF); (c) rectangular matrix with triangular fibers (RMTF); (d) square matrix with circular fibers (SMCF); (e) square matrix with hexagonal fibers (SMHF); and (f) square matrix with triangular fibers (SMTF). The corresponding fiber volume fraction for each of these is:

Table 1.1 Material properties

Material	Carbon fiber	Epoxy resin
Young's modulus	294 GPa	2.415 GPa
Poisson's ratio	0.3	0.35

RMCF = 0.13089; RMHF = 0.14433; RMTF = 0.08333;
SMCF = 0.08726; SMHF = 0.09622; SMTF = 0.05555.

Figure 1.4 shows the geometrical configuration of the unit cell used. It is obvious from Figure 1.4 that: (a) total area is 6 for RM and 9 for SM; and (b) the fiber's area is $\pi r^2 = 0.78539$ for circular fiber, $3^{3/2}t^2/2 = 3^{3/2} \times 0.57735^2/2 = 0.86602$ for hexagonal fiber, and 0.5 for triangular fiber. The fiber volume fraction listed above is obtained based on these data. The finite element meshes used in the calculation are shown in Figure 1.5.

The FE results obtained are listed in Table 1.2 and also shown in Figures 1.6–1.8. A comparison of the results between FEA and MMA for E_1 yield quite similar results. The average error between these results is within 3%, for all results, in determination of E_1. It indicates that MMA can provide acceptable accurate results for E_1. Figure 1.6 shows a comparison between the result E_1 of varying fiber and matrix geometries. Figures 1.7 and 1.8 list the comparison in results between E_2 and G_{12}, respectively,

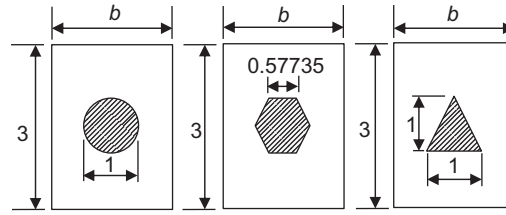

Figure 1.4 Geometrical configurations of matrix and fiber ($b = 2$ for RM and $b = 3$ for SM).

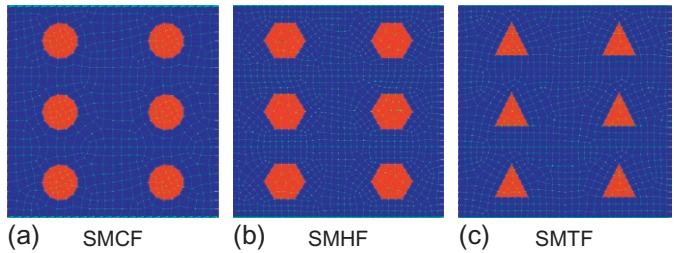

Figure 1.5 Finite element meshes for square matrix with different fiber geometries. (a) SMCF, (b) SMHF, and (c) SMTF.

Table 1.2 Composite's properties for carbon fiber with epoxy resin

Properties	E_1 (GPa)		E_2 (GPa)		G_{12} (GPa)	
Approach	MMA	FEA	MMA	FEA	MMA	FEA
RMCF	40.583	38.923	2.775	3.021	1.028	1.034
RMHF	44.502	43.743	2.818	3.145	1.044	1.062
RMTF	26.714	23.764	2.633	2.846	0.975	0.991
SMCF	27.861	26.351	2.644	2.774	0.979	0.991
SMHF	30.473	29.640	2.670	2.845	0.989	1.021
SMTF	18.614	18.710	2.556	2.736	0.947	0.994

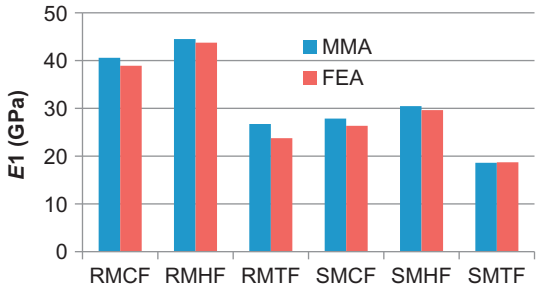

Figure 1.6 Comparison of E_1 results from FEA with those from MMA in the case of carbon fiber/epoxy resin.

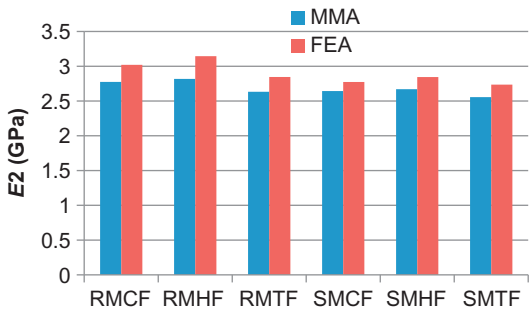

Figure 1.7 Comparison of E_2 results from FEA with those from MMA in the case of carbon fiber/epoxy resin.

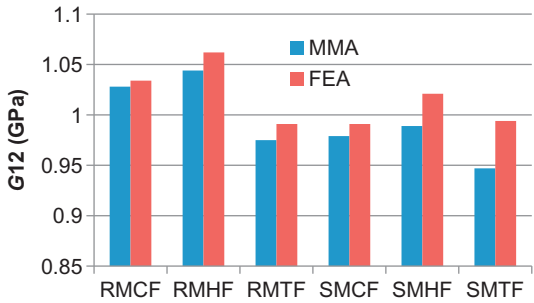

Figure 1.8 Comparison of G_{12} results from FEA with those from MMA in the case of carbon fiber/epoxy resin.

derived through MMA and FEA. The difference of these results is within 8%, between all the results collected for E_2 and G_{12}. As revealed by the graph, the difference in results is not always constant. The square matrix with circular fibers, for example, has a smaller difference than the other models between MMA and FEA results. This highlights the nonlinear nature of FEA modeling software. Another point to note is that the values obtained for E_1 using FEA are lower than those from MMA, while the values obtained for E_2 and G_{12} using FEA are higher than those from MMA. This is a result of the model thickness or the length in the fiber direction.

1.4.3 Direct homogenization

Direct homogenization is based on the average of local fields to calculate effective material properties. For instance, a uniform strain is applied to a fiber-reinforced composite and the average of the elastic displacement is calculated. Then one can calculate the effective material coefficients of the composite. In general, the local fields can be calculated by a numerical method, such as boundary element method (BEM) (Qin, 2004b) or FEM (Qin and Yang, 2008; Qin, 2000).

The constitutive equation used in direct method can be written as

$$\boldsymbol{\sigma} = \mathbf{E}\boldsymbol{\varepsilon} \tag{1.23}$$

where $\boldsymbol{\sigma}$, $\mathbf{E}$, and $\boldsymbol{\varepsilon}$ are, respectively, generalized stress, stiffness, and strain tensors. In direct method, $\boldsymbol{\varepsilon}$ and $\boldsymbol{\sigma}$ are averaged first, then the effective stiffness properties are obtained. In detail, for a heterogeneous medium, consider an RVE subjected to a specific boundary condition and calculate the local fields, $\boldsymbol{\varepsilon}$ and $\boldsymbol{\sigma}$, by a numerical method, such as FEM. Then a volume averaging is carried out and homogenized fields, $\overline{\boldsymbol{\varepsilon}}$ and $\overline{\boldsymbol{\sigma}}$, are obtained by

$$\overline{\boldsymbol{\varepsilon}} = \frac{1}{V}\int_{\Omega} \boldsymbol{\varepsilon} \mathrm{d}\Omega, \quad \overline{\boldsymbol{\sigma}} = \frac{1}{V}\int_{\Omega} \boldsymbol{\sigma} \mathrm{d}\Omega \tag{1.24}$$

The effective stiffness $\bar{\mathbf{E}}$ can be determined by

$$\overline{\boldsymbol{\sigma}} = \overline{\mathbf{E}}\,\overline{\boldsymbol{\varepsilon}} \tag{1.25}$$

Expanding Eq. (1.25), one can obtain

$$\overline{\sigma}_i = \overline{E}_{ij}\overline{\varepsilon}_j \tag{1.26}$$

Applying uniaxial $\overline{\varepsilon}_1 = 1$ and other $\overline{\varepsilon}_i = 0$ on the right-hand-side vector $\overline{\boldsymbol{\varepsilon}}$ and calculating all $\overline{\varepsilon}_i$ of the left-hand-side vector $\overline{\boldsymbol{\sigma}}$, one can obtain the effective stiffness coefficients $\bar{E}_{i1}$. The remaining $\bar{E}_{ij}$ can be obtained similarly.

1.4.4 Indirect homogenization

Indirect homogenization here refers to various homogenization methods derived from the generalized Eshelby's inclusion theory in which an elastic solution has been obtained for a single inclusion embedded in infinite elastic medium (Qin and Yang, 2008; Qin et al., 1998). Such a method is not involved in the calculation of average fields. A self-consistent scheme, a generalized self-consistent scheme, the Mori–Tanaka method, and a differential method are developed along this routine. The indirect methods have been widely used to predict the effective properties of composites (Yu and Qin, 1996; Qin and Yu, 1997, 1998). This section, however, is based on the developments in Qin and Yang (2008).

The effective properties that are represented by the effective stiffness $\bar{\mathbf{E}}$ or compliance $\overline{\mathbf{F}}$ of the composites, according to the average stress and strain, can be defined by Eq. (1.25) or

$$\overline{\boldsymbol{\varepsilon}} = \overline{\mathbf{F}}\overline{\boldsymbol{\sigma}} \tag{1.27}$$

The homogeneous boundary conditions are usually used to determine the overall material properties. For homogeneous traction $\boldsymbol{\sigma}^{\infty}$ on the boundary of an RVE, we have

$$\overline{\boldsymbol{\sigma}} = \boldsymbol{\sigma}^{\infty} \tag{1.28}$$

and

$$\overline{\boldsymbol{\varepsilon}} = \overline{\mathbf{F}}\boldsymbol{\sigma}^{\infty} \tag{1.29}$$

Thus, to find the effective compliance $\overline{\mathbf{F}}$, the average strain $\overline{\boldsymbol{\varepsilon}}$ must be computed for a composite subjected to a homogeneous traction boundary condition.

For homogeneous strain condition $\boldsymbol{\varepsilon}^{\infty}$ on the boundary of the RVE, one has

$$\overline{\boldsymbol{\varepsilon}} = \boldsymbol{\varepsilon}^{\infty}, \quad \overline{\boldsymbol{\sigma}} = \overline{\mathbf{E}}\boldsymbol{\varepsilon}^{\infty} \tag{1.30}$$

Accordingly, to determine $\bar{\mathbf{E}}$, the average stress $\overline{\boldsymbol{\sigma}}$ must be computed for a heterogeneous material subjected to a homogeneous strain boundary condition.

It is worthwhile to note that the volume average of stress and strain can be expressed in terms of phase volume fractions. For a general function G, the volume average can be written as

$$\begin{aligned} \overline{G} &= \frac{1}{V}\int_{\Omega} G\mathrm{d}\Omega = \frac{1}{V}\left[\int_{\Omega_1} G\mathrm{d}\Omega + \int_{\Omega_2} G\mathrm{d}\Omega + \cdots\right] \\ &= \frac{V_1}{V}\overline{G}^{(1)} + \frac{V_2}{V}\overline{G}^{(2)} + \cdots = v_1\overline{G}^{(1)} + v_2\overline{G}^{(2)} + \cdots \end{aligned} \tag{1.31}$$

where $\Omega_1, \Omega_2, \ldots (\Omega_1 + \Omega_2 + \cdots = \Omega)$ are subdomains that represent the domains occupied by phase $1, 2, \ldots$ of the composite material, and $V_1, V_2, \ldots$ are their volumes, while

$$v_1 = \frac{V_1}{V}, v_2 = \frac{V_2}{V}, \ldots \tag{1.32}$$

are referred to as volume fractions of the corresponding phases and $v_0 + v_1 + v_2 + \cdots = 1$. For an n-phase composite, the stress and strain can be expressed by

$$\overline{\boldsymbol{\sigma}} = \sum_{i=0}^{n-1} v_i \overline{\boldsymbol{\sigma}}^{(i)} \tag{1.33a}$$

$$\overline{\boldsymbol{\varepsilon}} = \sum_{i=0}^{n-1} v_i \overline{\boldsymbol{\varepsilon}}^{(i)} \tag{1.33b}$$

where the superscript (i) corresponds with phase i, and phase 0 ($i = 0$) refers to matrix.

The stress or strain in an inclusion is uniform when the inclusion shape is ellipsoidal. In this case, the effective properties can be expressed by so-called concentration factor of the stress or strain. It is assumed that the Hooke's law holds in each elastic phase

$$\boldsymbol{\sigma}^{(r)} = \mathbf{E}^{(r)} \boldsymbol{\varepsilon}^{(r)}, \quad (r = 0, 1, \ldots, n-1) \tag{1.34a}$$

$$\boldsymbol{\varepsilon}^{(r)} = \mathbf{F}^{(r)} \boldsymbol{\sigma}^{(r)}, \quad (r = 0, 1, \ldots, n-1) \tag{1.34b}$$

Substituting Eq. (1.34a) into Eq. (1.33a), and using Eq. (1.25), yields

$$\overline{\mathbf{E}} = \mathbf{E}^0 + \sum_{r=1}^{n} v_r \left(\mathbf{E}^{(r)} - \mathbf{E}^0 \right) \boldsymbol{\varepsilon}^{(r)} \overline{\boldsymbol{\varepsilon}}^{-1} \tag{1.35}$$

Substituting Eq. (1.34b) into Eq. (1.33b), and using Eq. (1.27), we have

$$\overline{\mathbf{F}} = \mathbf{F}^0 + \sum_{r=1}^{n} v_r \left(\mathbf{F}^{(r)} - \mathbf{F}^0 \right) \boldsymbol{\sigma}^{(r)} \overline{\boldsymbol{\sigma}}^{-1} \tag{1.36}$$

It is assumed that there are relations between average strain and local strain

$$\boldsymbol{\varepsilon}^{(r)} = \mathbf{A}^r \overline{\boldsymbol{\varepsilon}} \tag{1.37}$$

Similarly, the average stress and local stress have the relation

$$\boldsymbol{\sigma}^{(r)} = \mathbf{B}^r \overline{\boldsymbol{\sigma}} \tag{1.38}$$

Thus, the effective stiffness $\overline{\mathbf{c}}$ and compliance $\overline{\mathbf{f}}$ of the composite can be written as

$$\overline{\mathbf{E}} = \mathbf{E}^0 + \sum_{r=1}^{n} v_r \left(\mathbf{E}^{(r)} - \mathbf{E}^0 \right) \mathbf{A}^r \tag{1.39}$$

$$\overline{\mathbf{F}} = \mathbf{F}^0 + \sum_{r=1}^{n} v_r \left(\mathbf{F}^r - \mathbf{F}^0 \right) \mathbf{B}^r \tag{1.40}$$

where $\mathbf{A}^r$ and $\mathbf{B}^r$ are referred to as concentration factors of stress and strain, respectively. They are functions in terms of the properties of the constituents and the shape of inclusions.

1.4.4.1 Self-consistent scheme

In the self-consistent scheme, the effect of inclusion interaction is taken into account approximately by embedding each inclusion directly in the effective medium. In other words, it is assumed that a typical inclusion (fiber, particle, or microvoid) is embedded in an infinite effective medium subjected to a uniform strain $\boldsymbol{\varepsilon}^{\infty}$ at infinite boundary. The corresponding effective stress is then written as

$$\overline{\boldsymbol{\sigma}} = \overline{\mathbf{E}} \boldsymbol{\varepsilon}^{\infty} \tag{1.41}$$

The strain in the inclusion consists of two parts, uniform strain $\boldsymbol{\varepsilon}^{\infty}$ and a perturbing strain $\boldsymbol{\varepsilon}^{\mathrm{pt}}$, and the corresponding stress in the inclusion is $\overline{\boldsymbol{\sigma}} + \boldsymbol{\sigma}^{\mathrm{pt}}$, that is

$$\boldsymbol{\varepsilon}^{(1)} = \overline{\boldsymbol{\varepsilon}} + \boldsymbol{\varepsilon}^{\mathrm{pt}} \tag{1.42}$$

$$\boldsymbol{\sigma}^{(1)} = \overline{\boldsymbol{\sigma}} + \boldsymbol{\sigma}^{\mathrm{pt}} \tag{1.43}$$

where superscript (1) refers to the inclusion.

Using equivalent inclusion principle and the assumption of self-consistent method, yields

$$\overline{\boldsymbol{\sigma}} + \boldsymbol{\sigma}^{\mathrm{pt}} = \mathbf{E}^{(1)} \left(\overline{\boldsymbol{\varepsilon}} + \boldsymbol{\varepsilon}^{\mathrm{pt}} \right) = \overline{\mathbf{E}} \left(\overline{\boldsymbol{\varepsilon}} + \boldsymbol{\varepsilon}^{\mathrm{pt}} - \boldsymbol{\varepsilon}^{*} \right) \tag{1.44}$$

and

$$\boldsymbol{\varepsilon}^{\mathrm{pt}} = \mathbf{S} \boldsymbol{\varepsilon}^{*} \tag{1.45}$$

where $\mathbf{S}$ is Eshelby tensor and $\boldsymbol{\varepsilon}^{*}$ is equivalent to eigenstrain.

Solving Eqs. (1.42)–(1.44), yields

$$\boldsymbol{\varepsilon}^{(1)} = \left[\mathbf{I} + \mathbf{S}\overline{\mathbf{E}}^{-1}\left(\mathbf{E}^{(1)} - \overline{\mathbf{E}}\right)\right]^{-1}\overline{\boldsymbol{\varepsilon}} \tag{1.46}$$

where $\mathbf{I}$ is unit tensor. A comparison of Eq. (1.46) with Eq. (1.37) yields the strain concentration factor as

$$\mathbf{A}^{(1)} = \left[\mathbf{I} + \mathbf{S}\overline{\mathbf{E}}^{-1}\left(\mathbf{E}^{(1)} - \overline{\mathbf{E}}\right)\right]^{-1} \tag{1.47}$$

The effective properties can be found by substituting Eq. (1.47) in Eq. (1.39). It should be mentioned that the strain concentration factor is a function of unknown effective stiffness $\bar{\mathbf{E}}$. An iteration procedure is required to solve Eq. (1.39) for the effective properties.

1.4.4.2 Mori–Tanaka method

Consider a finite-fraction inclusion problem with eigenstrain $\boldsymbol{\varepsilon}^*$. With the Mori–Tanaka method, the average stress can be expressed as

$$\langle\boldsymbol{\sigma}\rangle_m = \mathbf{E}^{(0)}\langle\boldsymbol{\varepsilon}\rangle_m = -v_1\mathbf{E}^{(0)}(\mathbf{S}\boldsymbol{\varepsilon}^* - \boldsymbol{\varepsilon}^*) \tag{1.48}$$

where $\langle\boldsymbol{\varepsilon}\rangle_m$ is average strain in the matrix, and v_1 is volume fraction of inclusion.

For a binary composite subjected to homogeneous boundary condition (1.28), denoting $r=0$ matrix and $r=1$ inclusion, the effective stress is $\boldsymbol{\sigma}^\infty$. For the same shaped pure matrix applied to the same boundary condition, the corresponding strain $\boldsymbol{\varepsilon}^\infty$ can be expressed by

$$\boldsymbol{\sigma}^\infty = \mathbf{E}^0\boldsymbol{\varepsilon}^\infty \tag{1.49}$$

where $\mathbf{E}^0$ is the stiffness of the matrix. Due to the presence of inclusion, the strain in real matrix of the composite differs from one in pure matrix. Denote $\widetilde{\boldsymbol{\varepsilon}}$ as the perturbing strain and $\widetilde{\boldsymbol{\sigma}}$ as the corresponding perturbing stress. Thus, $\boldsymbol{\varepsilon}^\infty + \widetilde{\boldsymbol{\varepsilon}}$ and $\boldsymbol{\sigma}^\infty + \widetilde{\boldsymbol{\sigma}}$ are strain and stress in real matrix with

$$\boldsymbol{\sigma}^\infty + \widetilde{\boldsymbol{\sigma}} = \mathbf{E}^0(\boldsymbol{\varepsilon}^\infty + \widetilde{\boldsymbol{\varepsilon}}) \tag{1.50}$$

The strain and stress in the inclusion are different from ones in the matrix. The differences are $\boldsymbol{\varepsilon}'$ and $\boldsymbol{\sigma}'$, respectively. Thus $\boldsymbol{\varepsilon}^\infty + \widetilde{\boldsymbol{\varepsilon}} + \boldsymbol{\varepsilon}'$ and $\boldsymbol{\sigma}^\infty + \widetilde{\boldsymbol{\sigma}} + \boldsymbol{\sigma}'$ are the strain and stress in the inclusion. The equivalent inclusion principle yields:

$$\boldsymbol{\sigma}^{(1)} = \boldsymbol{\sigma}^\infty + \widetilde{\boldsymbol{\sigma}} + \boldsymbol{\sigma}' = \mathbf{E}^1(\boldsymbol{\varepsilon}^\infty + \widetilde{\boldsymbol{\varepsilon}} + \boldsymbol{\varepsilon}') = \mathbf{E}^0(\boldsymbol{\varepsilon}^\infty + \widetilde{\boldsymbol{\varepsilon}} + \varepsilon' - \boldsymbol{\varepsilon}^*) \tag{1.51}$$

$$\boldsymbol{\varepsilon}' = \mathbf{S}\boldsymbol{\varepsilon}^* \tag{1.52a}$$

$$\widetilde{\boldsymbol{\varepsilon}} = -v_1(\mathbf{S} - \mathbf{I})\boldsymbol{\varepsilon}^* \tag{1.52b}$$

Equation (1.52b) is obtained based on the Mori–Tanaka's concept of average stress, in Eq. (1.48). Solving Eq. (1.51) yields

$$\boldsymbol{\varepsilon}^{*} = \mathbf{H}\boldsymbol{\varepsilon}^{\infty} \tag{1.53}$$

where $\mathbf{H} = \left[\mathbf{E}^{0} + \Delta\mathbf{E}(v_1\mathbf{I} - v_0\mathbf{S})\right]^{-1}\Delta\mathbf{E}$, $\Delta\mathbf{E} = \mathbf{E}^{1} - \mathbf{E}^{0}$, and $v_0 = 1 - v_1$ is the volume fraction of matrix.

Accordingly, the effective strain $\overline{\boldsymbol{\varepsilon}}$ is

$$\begin{aligned}\overline{\boldsymbol{\varepsilon}} = (1-v_1)\boldsymbol{\varepsilon}^{(0)} + v_1\boldsymbol{\varepsilon}^{(1)} &= (1-v_1)(\boldsymbol{\varepsilon}^{\infty} + \widetilde{\boldsymbol{\varepsilon}}) + v_1(\boldsymbol{\varepsilon}^{\infty} + \widetilde{\boldsymbol{\varepsilon}} + \boldsymbol{\varepsilon}') \\ &= \boldsymbol{\varepsilon}^{\infty} + v_1\boldsymbol{\varepsilon}^{*} = (\mathbf{I} + v_1\mathbf{H})\boldsymbol{\varepsilon}^{\infty}\end{aligned} \tag{1.54}$$

The effective stiffness of the composite is then given by

$$\overline{\mathbf{E}} = \mathbf{E}^{0}(\mathbf{I} + v_1\mathbf{H})^{-1} \tag{1.55}$$

1.4.4.3 Differential method

The essence of the differential scheme, an incremental form of the self-consistent method, is the construction of the final defected medium from the intact material through successive replacement of an incremental area of the current defected material with that of the inclusions. Denote $\bar{\mathbf{E}}$ as the effective stiffness of composite with volume V_0 and inclusion volume fraction v_1. Add volume δV of inclusion to the composite so that inclusion volume fraction is $v_1 + \delta v_1$ and the effective stiffness is $\overline{\mathbf{E}} + \delta\overline{\mathbf{E}}$. To keep a constant volume V_0 of the composite, the volume of composite is detracted by δV before adding the inclusion. Thus concentration of the inclusion is

$$v_1 V_0 + \delta V - v_1\delta V = (v_1 + \delta v_1)V_0 \tag{1.56}$$

It is rearranged as

$$\frac{\delta V}{V} = \frac{\delta v_1}{1 - v_1} \tag{1.57}$$

The average stress is

$$\overline{\boldsymbol{\sigma}} = \left(\overline{\mathbf{E}} + \delta\overline{\mathbf{E}}\right)\overline{\boldsymbol{\varepsilon}} \tag{1.58}$$

Then one has

$$\overline{\boldsymbol{\varepsilon}} = \frac{V_0 - \delta V}{V_0}\boldsymbol{\varepsilon} + \frac{\delta V}{V_0}\boldsymbol{\varepsilon}^{(1)}, \quad \overline{\boldsymbol{\sigma}} = \frac{V_0 - \delta V}{V_0}\boldsymbol{\sigma} + \frac{\delta V}{V_0}\boldsymbol{\sigma}^{(1)} \tag{1.59}$$

where $\boldsymbol{\sigma}$ and $\boldsymbol{\varepsilon}$ denote the average stress and strain in instantaneous composite, respectively. $\boldsymbol{\sigma}^{(1)}$ and $\boldsymbol{\varepsilon}^{(1)}$ represent the average stress and strain of the added inclusion, respectively. Because the added inclusion is very small, the strain concentration factor can be calculated by Eshelby's solution of a dilute inclusion problem

$$\boldsymbol{\varepsilon}^{(1)} = \mathbf{A}\overline{\boldsymbol{\varepsilon}} \tag{1.60}$$

where $\mathbf{A} = \left[\mathbf{I} + \mathbf{S}\overline{\mathbf{E}}^{-1}\left(\mathbf{E}^1 - \overline{\mathbf{E}}\right)\right]^{-1}$.

Substituting Eqs. (1.59) and (1.60) into Eq. (1.58), yields

$$\delta\overline{\mathbf{E}} = \left(\mathbf{E}^1 - \overline{\mathbf{E}}\right)\mathbf{A}\frac{\delta V}{V_0} \tag{1.61}$$

Using Eq. (1.57), and setting $\delta v_1 \to 0$, we can obtain

$$\frac{\mathrm{d}\mathbf{E}}{\mathrm{d}v_1} = \frac{1}{1 - v_1}\left(\mathbf{E}^1 - \mathbf{E}\right)\mathbf{A} \tag{1.62}$$

This is a differential equation about effective stiffness. Its initial condition is

$$\overline{\mathbf{E}}\big|_{v_1 = 0} = \mathbf{E}^0 \tag{1.63}$$

Equation (1.62) is a nonlinear equation that can be solved by a numerical procedure.

1.4.5 Micromechanics-boundary element mixed approach

It is noted that common to each of the micromechanics theories described in Section 1.4.4 is the use of the well-known stress and strain concentration factors obtained through an analytical solution of a single crack, void, or inclusion embedded in an infinite medium. However, for a problem with complexity in the aspects of geometry and mechanical deformation, a combination of these micromechanics approaches and numerical methods such as the FEM and BEM presents a powerful computational tool for estimating effective material properties. It is also noted from Section 1.4.4 that the estimation of the average strain (or stress), which may be expressed in terms of integral equations contains unknown variables on the boundary only, is the key to predicting the concentration factor $\mathbf{A}_2$ (or $\mathbf{B}_2$). Therefore, BEM is very suitable for performing this type of calculation. In this section, a micromechanics-BE mixed algorithm reported in Qin (2004a,b) for analyzing the effective behavior of piezoelectric composites is described. The algorithm is based on a typical micromechanics model (self-consistent) and a two-phase BE formulation. An iteration scheme is designated for the self-consistent-BE mixed method.

1.4.5.1 BE formulation for two-phase composites

In this section, a two-phase BE model is introduced for displacements and stresses on the boundary of the subdomain of each phase (Qin and Yang, 2008; Qin, 2004a; Yang and Qin, 2004). The two subdomains are separated by the interfaces between inclusion

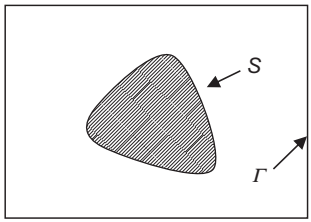

Figure 1.9 RAE used in BE analysis.

and matrix (see Figure 1.9). Each subdomain can be separately modeled by direct BEM. Global assembly of the BE subdomains is then performed by enforcing continuity of the displacements and stresses at the subdomain interface.

In two-dimensional linear elasticity, the BE formulation takes the form (Qin, 1993, 1998, 2009):

$$c^{(\alpha)}(\boldsymbol{\xi})u_i^{(\alpha)}(\boldsymbol{\xi}) = \int_{S^{(\alpha)}} \left[U_{ij}^{(\alpha)}(\mathbf{x},\boldsymbol{\xi})T_j^{(\alpha)}(\mathbf{x}) - F_{ji}^{(\alpha)}(\mathbf{x},\boldsymbol{\xi})u_j^{(\alpha)}(\mathbf{x})\right] \mathrm{d}S(\mathbf{x}) \tag{1.64}$$

where u_i and $T_i = \sigma_{ij}n_j$ are, respectively, the displacement and boundary traction in i direction with n_j being the component of the unit outward normal to the boundary, superscript (α) stands for the quantity associated with the αth phase ($\alpha = 1$ being matrix and $\alpha = 2$ being inclusion) and

$$S^{(\alpha)} = \begin{cases} S+\Gamma & \alpha = 1 \\ S & \alpha = 2 \end{cases}, \quad c^{(\alpha)}(\boldsymbol{\xi}) = \begin{cases} 1 & \text{if } \boldsymbol{\xi} \in \Omega^{(\alpha)} \\ 0.5 & \text{if } \boldsymbol{\xi} \in S^{(\alpha)} \left(S^{(\alpha)} \text{ smooth}\right) \\ 0 & \text{if } \boldsymbol{\xi} \notin \Omega^{(\alpha)} \cup S^{(\alpha)} \end{cases} \tag{1.65}$$

For plane strain, the integral kernels G_{ij} and F_{ij} are given by Qin (1998) and Qin and Huang (1990)

$$U_{ij}^{(\alpha)}(\mathbf{x},\boldsymbol{\xi}) = \frac{1}{8\pi G^{(\alpha)}(1-\mu^{(\alpha)})}\left[\left(3-4\mu^{(\alpha)}\right)\ln\left(\frac{1}{r}\right)\delta_{ij} + \frac{r_i r_j}{r^2}\right] \tag{1.66}$$

$$F_{ji}^{(\alpha)}(\mathbf{x},\boldsymbol{\xi}) = -\frac{1}{4\pi(1-\mu^{(\alpha)})r}\left(1-2\mu^{(\alpha)}\right)\left(n_j\frac{r_i}{r} - n_i\frac{r_j}{r}\right) + \left[\left(1-2\mu^{(\alpha)}\right)\delta_{ij} + \frac{2r_i r_j}{r^2}\right]\frac{r_n}{r} \tag{1.67}$$

with

$$r_i = x_i - \xi_i, \quad r_n = r_i n_i, \quad r = \sqrt{r_i r_i} \tag{1.68}$$

Equations (1.66) and (1.67) can be used for plane stress if $\mu^{(\alpha)}$ is replaced by $\mu^{(\alpha)}\left(1-\mu^{(\alpha)}\right)$.

To obtain a weak solution of Eq. (1.64) as in the conventional BEM, the boundary $S^{(\alpha)}$ is divided into a series of boundary elements. After performing discretization

using various kinds of boundary elements (e.g., constant element, linear element, higher-order element) and collecting the unknown terms to the left-hand side and the known terms to the right-hand side as well as using continuity conditions at the interface S (Figure 1.9), the boundary integral Eq. (1.64) becomes a set of linear algebraic equations:

$$\mathbf{KY} = \mathbf{P} \tag{1.69}$$

where $\mathbf{Y}$ and $\mathbf{P}$ are the total unknown and known vectors, respectively, and $\mathbf{K}$ is the known coefficient matrix.

1.4.5.2 Algorithm for self-consistent approach

As stated in Section 1.4.4.1, in the self-consistent method, for each inclusion, the effect of inclusion interaction is taken into account approximately by embedding each inclusion in the effective medium whose properties are unknown. In this case, the material constants appearing in the boundary element formulation (1.64) are unknown. Consequently a set of initial trial values of the effective properties is needed and an iteration algorithm is required. In detail, for the algorithm:

(a) Assume initial values of material constants $\bar{\mathbf{E}}_{(0)}$.
(b) Solve Eq. (1.69) for the displacement u_j using the values of $\overline{\mathbf{E}}_{(i-1)}$, where the subscript (i) stands for the variable associated with the ith iterative cycle. Calculate the average strains using the current values of u_j.
(c) Calculate $\mathbf{A}_i^{(1)}$ in Eq. (1.47) by way of Eq. (1.37) using the current values of average strain, and then determine $\bar{\mathbf{E}}_{(i)}$ by way of Eq. (1.47).
(d) If $\delta_{(i)} = \left\|\overline{\mathbf{E}}_{(i)} - \overline{\mathbf{E}}_{(i-1)}\right\| / \left\|\overline{\mathbf{E}}_{(0)}\right\| \leq \delta$, where δ is a convergent tolerance, terminate the iteration; otherwise take $\bar{\mathbf{E}}_{(i)}$ as the initial value and go to step (b).

1.4.6 Periodic boundary conditions in unit cell scheme

From a practical point of view, it is regarded that the composite material is an assembly of periodic unit cells (Figure 1.10). A unit cell is an RVE, as shown in Figure 1.10.

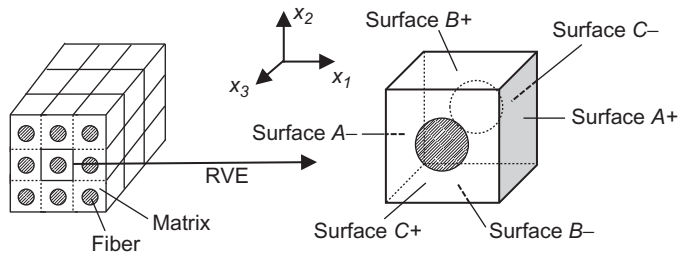

Figure 1.10 Schematic diagrams of periodic 1–3 composite laminate (a) and unit cell (b) (the fiber laminates are poled in x_3 direction) (Berger et al., 2005).

1.4.6.1 Periodic boundary condition

For the statistically homogeneous medium consisting of periodic unit cells (Figure 1.10), periodic boundary conditions are required to apply on the boundaries of the RVE. The general periodic conditions expressed by Havner (1971) can be applied to ensure periodic displacement and subsequent stress field.

$$\begin{aligned} u_i(y) &= u_i(y+Y) \\ \sigma_{ij}(y) &= \sigma_{ij}(y+Y) \end{aligned} \quad (i,j=1,2,3) \tag{1.70}$$

where σ_{ij} denotes the stress components in three-dimensions respectively, y represents any point in the periodic domain and Y, the periodicity. Applying this displacement condition to the boundary of the unit cell in Figure 1.10 yields

$$u_i^{j+} = u_i^{j-} \quad (i,j=1,2,3) \tag{1.71}$$

which means that the three-dimensional displacement vector for any pair of corresponding locations on areas $A-/A+$, $B-/B+$, and $C-/C+$ should be the same. A more explicit periodic boundary condition is then given as (Qin and Yang, 2008)

$$u_i = \overline{S}_{ij}x_j + v_i \tag{1.72}$$

where the average strain $\overline{S}_{ij}$ is included as an arbitrarily imposed constant strain; v_i denotes the periodic part of displacement component, which depends on the global loadings.

Based on the boundary condition (Eq. 1.72), Xia et al. (2003) and Berger et al. (2005) developed a unified periodic boundary condition:

$$u_i^{j+}(x,y,z) - u_i^{j-}(x,y,z) = c_i^j \quad (i,j=1,2,3) \tag{1.73}$$

where the constant terms c_1^1, c_2^2, and c_3^3 represent the normal loads that are either traction or compression; while, $c_1^2 = c_2^1$, $c_1^3 = c_3^1$, and $c_2^3 = c_3^2$ represent the in-plane shear load.

1.4.6.2 FE modeling

Element type and material property

To show the application of the periodic boundary condition in FE modeling, the SOLID226 in ANSYS element library is used in the following analysis, which is a 20-node hexagonal shaped element type with 3D displacement degree-of-freedom (DoF) and additional voltage DoF. This element type is easy for the implementation of periodic boundary conditions.

The material properties inputs are based on Berger et al. (2005) and listed in Table 1.3 for the reader's convenience.

Table 1.3 **Composite constituent's properties (Berger et al., 2005)**

	c_{11} (10^{10})	c_{12} (10^{10})	c_{13} (10^{10})	c_{33} (10^{10})	c_{44} (10^{10})	c_{66} (10^{10})	e_{15}	e_{31}	e_{33}	κ_{11} (10^{-9})	κ_{33} (10^{-9})
PZT-5	12.1	7.54	7.52	11.1	2.11	2.28	12.3	5.4	15.8	8.11	7.35
Polymer	0.386	0.257	0.257	0.386	0.064	0.064	—	—	—	0.07965	0.07965

Element mesh

For meshing, the area geometry is generated first and then sweep mesh is used to further generate the volume. In this way, the meshing result on $C+/C-$ is the same. In addition, with the setting of the RVE edge line divisions, meshing results on $A+/A-$ and $B+/B-$ are also the same. Ultimately, this provides explicit convenience to imposing periodic boundary conditions. As illustrated, when dealing with the situation when volume fraction is specified, say 0.666, the outline of the fiber circle is much closer to the RVE edge; in this case, a lower density of element as shown in Figure 1.11a is not sufficient for accurate analysis since the elements between the boundary of the RVE and the fiber have been lessened and shown distortion. When the edge division is 40 indicated in Figure 1.11b, the meshing quality is significantly improved.

As for periodic boundary condition, specific boundary conditions will be assigned to the exact opposite positions, namely $A+/A-$, $B+/B-$, and $C+/C-$. For example, in x-direction

$$u_i\left(x^{A+}, y_j, z_j\right) - u_i\left(x^{A-}, y_k, z_k\right) = c \quad (i = 1,2,3) \tag{1.74}$$

where subscripts j and k are the nodal number of any pair of nodes on opposite locations, $A+$ and $A-$ area, respectively.

The boundary conditions are shown in Figure 1.12.

Since the meshing scheme has ensured that there exists a pair of corresponding nodes at the opposite positions, the problem lies in developing a method to apply constraint equations on each pair of node for overcoming the problem of time-consuming over the node pair selection by graphical users' interface. An internal program has thus been designed for accomplishing the task. The procedures for the implementation are described as follows:

(a) Define the area $A+$, $B+$, and $C+$ as master areas, while $A-$, $B-$, and $C-$ as slave areas. Establish two arrays containing the node number (j, k) and coordinates ($y_{j,k}$, $z_{j,k}$) of each node (the x coordinate is not necessary, because the nodes are located on $A+$ and $A-$ areas where the x coordinate is a constant).

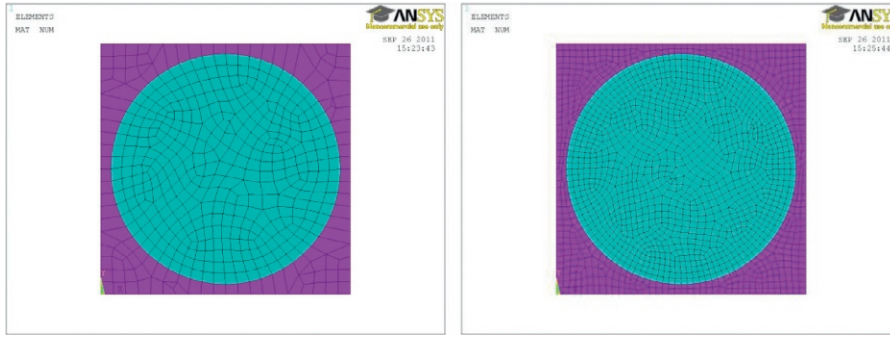

Figure 1.11 Different meshing density when volume fraction is 0.666. The RVE edge line is set into (a) 20 and (b) 40 divisions.

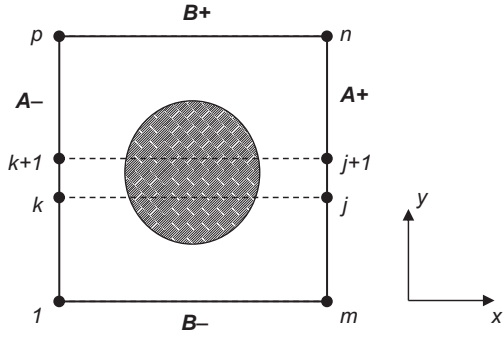

Figure 1.12 Application of periodic boundary conditions from a coordinate's view.

(b) Start from the first node in master array; get the node number j;
(c) Use the coordinates (y_j, z_j) of the node j to find the node at the exact opposite location, $y_j = y_k$; $z_j = z_k$; and select the node k from the slave array.
(d) Given the node number of the nodes on opposite location, constraint equations could be established.

The same procedures are applied on $B+/B-$ and $C+/C-$ areas, while the coordinates obtained and stored will be X/Z and X/Y, respectively.

When integrating the constraint equations in three directions, special care has been taken to avoid over-constraint over the edges that connect areas $A+/A-$, $B+/B-$, and $C+/C-$. Over-constraint may occur when the DoF of one node is specified more than once. For example, when applying $x-y$ in-plane shear load via constraint equations as shown in Figure 1.13, based on the periodic boundary conditions for $A+/A-$, the DoF relations between node 1 and 2 are $u_2 = u_1$ and $v_2 = v_1 + c$ while as to areas $B+/B-$, there will be relations between nodes 2 and 3 that $u_2 = u_3 + c$ and $v_2 = v_3$; the same situation will also occur in node 3. In this case, when applying constraint equations over $B+/B-$, the corner nodes of the RVE will be excluded to avoid over-constraint.

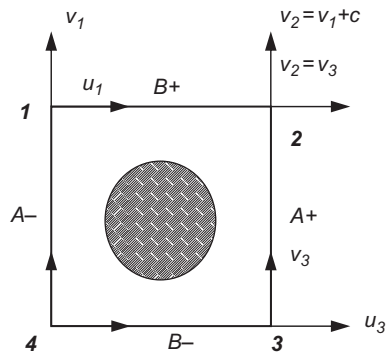

Figure 1.13 Over-constraint situations for a 2D model.

Numerical results

After applying appropriate boundary conditions to the RVE, the element stiffness matrix is integrated to form a global matrix, and the constitutive equations are solved to obtain the strain and stress field by ANSYS. To further clarify, for the arbitrary term in the periodic boundary conditions, when required, the imposed nodal displacement difference c is prescribed to be 0.1 mm and the imposed electric potential V is controlled to be 10 V. It is noted that when calculating the dielectric tensors, the relative permittivity factor of the free-space is constrained to be zero, rather than the default value, which is 8.85E−12 F/m. To maintain consistency, the units of the results listed in Tables 1.3 and 1.4 are N/m^2, C/m^2, and F/m, for elastic, piezoelectric, and dielectric tensors, respectively.

The effective coefficients for different fiber volume fraction are calculated using the same algorithm with the variation to the fiber radius. The results are listed in Table 1.4.

1.5 Toughening mechanisms of composites

Composite toughening could be made in many ways, such as transformation toughening, toughening by particle-induced shear bending, crack-deflection toughening, and crack bridging toughening. This section, however, focuses on matrix toughened by particulate materials. When a particulate second phase is introduced in a matrix, there are several toughening mechanisms, including crack front pinning, particle bridging, crack-path deflection, matrix cracking. Each of these mechanisms is briefly reviewed below.

1.5.1 Crack front pinning

As indicated in Pearson and Yee (1993), in this mechanism, the particles (rigid thermoplastic particles in particular) could act as impenetrable objectives that cause the crack to bow out, which consumes extra energy, if the difference in toughness between the brittle matrix and the ductile particles is large enough. Indirect evidence for the occurrence of this mechanism is the observation of "tails" near the particles on the fracture surface when viewed using SEM. The toughening effect due to this mechanism is evaluated by (Pearson and Yee, 1993; Lange, 1970)

$$\frac{G_{\mathrm{Ic}}}{G_0} = 1 + \frac{T}{d_{\mathrm{s}} G_0} \tag{1.75}$$

where G_{Ic} is the fracture toughness of the matrix modified by the particles, G_0 is the fracture toughness of the matrix unmodified by the particles, T is the line energy per unit crack front, and d_{s} is the center-to-center distance between particles:

$$d_{\mathrm{s}} = \frac{2d_{\mathrm{p}}(1-f)}{3f} \tag{1.76}$$

with d_{p} being the diameter of the particles and f the volume fraction of particles.

Table 1.4 Effective properties versus different volume fractions

	Fiber volume fraction					
	0.111	**0.222**	**0.333**	**0.444**	**0.555**	**0.666**
c_{11}	4.459E+09	5.301E+09	6.572E+09	8.399E+09	1.108E+10	1.632E+10
c_{12}	2.874E+09	3.222E+09	3.652E+09	4.135E+09	4.680E+09	5.883E+09
c_{13}	2.920E+09	3.367E+09	3.958E+09	4.780E+09	6.071E+09	8.493E+09
c_{33}	9.725E+09	1.584E+10	2.189E+10	2.851E+10	3.661E+10	4.327E+10
c_{44}	7.974E+08	9.925E+08	1.242E+09	1.600E+09	2.339E+09	3.298E+09
c_{66}	7.533E+08	8.781E+08	1.026E+09	1.230E+09	1.540E+09	2.163E+09
e_{13}	−2.903E−02	−6.643E−02	−1.166E−01	−1.878E−01	−2.986E−01	5.075E−01
e_{33}	2.410E+00	4.801E+00	7.199E+00	9.643E+00	1.198E+01	1.418E+01
e_{15}	9.465E−02	2.120E−01	3.620E−01	5.774E−01	1.021E+00	1.597E+00
κ_{11}	7.965E−11	7.965E−11	7.965E−11	7.965E−11	7.965E−11	7.965E−11
κ_{33}	1.066E−09	1.920E−09	2.844E−09	3.789E−09	4.703E−09	5.559E−09

1.5.2 Particle bridging or crack bridging

The mechanism of particle bridging is effective if the particles are perfectly bonded to the matrix and if the advancing crack tip is drawn to particles so that bridges are left behind. An explanation of toughening via crack bridging considers the energy consumed when the particles are plastically deformed and then torn. To evaluate the amount of toughness one can expect from the crack bridging, Ahmad et al. (1986) proposed a model for rubber-modified matrix based on the idea that improvements in toughness may be attributed solely to the stretching and tearing of rubber particles in the crack wake. Thus increase in toughness can be rationalized by considering the shielding effect, which is the reduction of the stress intensity factor K at the crack tip (Pearson and Yee, 1993):

$$\frac{K_c}{K_0} = \phi(1-f) + \frac{fE^*\Gamma_t}{2\phi(1-f)K_0^2} \tag{1.77}$$

where K_c is the fracture toughness of the rubber-modified matrix, K_0 is the fracture toughness of the unmodified matrix, ϕ is a correction factor that accounts for crack bowing, f is the volume fraction of rubber particles, E^* is the stiffness of the particle, and Γ_t is the tearing energy of the rubber particles. The model shows that improvements in toughness should be greater when larger particles are used.

Besides, crack bridging may occur by frictional interlocking of opposing fracture surfaces and by the formation of ligamentary bridges between them. Whiskers or fibers can also act as crack bridging sites like coarse grains (Bengisu and Inal, 1994).

1.5.3 Crack path deflection

Theoretically, crack-deflection toughening occurs whenever interactions between the crack front and a second-phase inclusion, such as particles, cause the crack to propagate out of plane, reducing the stress intensity factor at the crack tip, compared to self-similar planar crack growth. In other words, the energy required to propagate such a crack increases. The toughening mechanism for different inclusions was analyzed by Faber and Evans (1983) who proposed the following model:

$$\frac{K_c}{K_0} = \left(\frac{E_c}{E_0}(1+0.87f)\right)^{1/2} \tag{1.78}$$

where E_c is the Young's modulus of the modified matrix, and E_0 is the Young's modulus of the unmodified matrix. As indicated in Bengisu and Inal (1994), two conditions can lead to crack deflection: residual strain in the composite and weak matrix/second-phase interfaces. Residual strain can be generated by elastic modulus and/or thermal expansion mismatch between the matrix and second-phase anisotropy of thermal expansion in a monolithic or composite material.

1.5.4 Microcrack toughening

The idea behind the mechanism of microcrack toughening is that stable grain boundary microcracks are nucleated by the high stresses in the vicinity of the macroscopic crack tip. These microcracks then lower the stress experienced by the tip. This shielding effect has been studied from two vantage points: one involving a smearing out of the effects of the microcracks appropriate to a zone of profuse microcracking and the other treating the interaction of the macrotip with discrete microcracks (Hutchinson, 1989). Generally, microcrack toughening involves two types of crack shielding phenomena (Bengisu and Inal, 1994; Evans and Fu, 1985): one type is due to the reduced elastic modulus of the material upon microcracking; another and more important type is due to dilatation caused by microcracking. Hutchinson (1987) defined the elastic modulus contribution as

$$\frac{dK_c}{K_c} = \frac{\left(k_1 - \frac{5}{8}\right)\left(\frac{G}{G^*} - 1\right)\left(k_2 + \frac{3}{4}\right)\left(\frac{\mu^* G}{G^*} - \mu\right)}{1 - \mu} \tag{1.79}$$

where K_c is the toughness in the absence of microcracking, k_1 and k_2 are constants depending on the microcracking zone shape (Bengisu and Inal, 1994), G and G^* are shear moduli of the material before and after microcracking, respectively, and μ and μ^* represent Poisson's ratios before and after microcracking, respectively.

The dilatational contribution is given by (Bengisu and Inal, 1994):

$$dK_c = k_3 E \theta_T h^{1/2} \tag{1.80}$$

where k_3 is a constant that depends on the microcrack zone shape and size, E is the Young's modulus of the material before microcracking, θ_T is the dilatational strain caused by microcracking, and h is the process zone width.

References

Ahmad, Z.B., Ashby, M.F., Beaumont, P.W.R., 1986. The contribution of particle-stretching to the fracture-toughness of rubber modified polymers. Scr. Metall. 20, 843–848.

Antoniou, A.E., Kensche, C., Philippidis, T.P., 2009. Mechanical behavior of glass/epoxy tubes under combined static loading. Part II: validation of FEA progressive damage model. Compos. Sci. Technol. 69, 2248–2255.

Bao, G., Hutchinson, J.W., McMeeking, R.M., 1991. Particle reinforcement of ductile matrices against plastic-flow and creep. Acta Metall. Mater. 39, 1871–1882.

Bengisu, M., Inal, O.T., 1994. Whisker toughening of ceramics—toughening mechanisms, fabrication, and composite properties. Annu. Rev. Mater. Sci. 24, 83–124.

Berger, H., Kari, S., Gabbert, U., Rodriguez-Ramos, R., Guinovart, R., Otero, J.A., Bravo-Castillero, J., 2005. An analytical and numerical approach for calculating effective material coefficients of piezoelectric fiber composites. Int. J. Solids Struct. 42, 5692–5714.

Damiel, I.M., Ishai, O., 2006. Engineering Mechanics of Composite Materials. Oxford University Press, New York.
Evans, A.G., Fu, Y., 1985. Some effects of microcracks on the mechanical-properties of brittle solids. 2. Microcrack toughening. Acta Metall. 33, 1525–1531.
Faber, K.T., Evans, A.G., 1983. Crack deflection processes. 1. Theory. Acta Metall. 31, 565–576.
Feng, X.Q., Mai, Y.W., Qin, Q.H., 2003. A micromechanical model for interpenetrating multiphase composites. Comput. Mater. Sci. 28, 486–493.
Gasik, M.M., 1998. Micromechanical modelling of functionally graded materials. Comput. Mater. Sci. 13, 42–55.
Gibson, R.F., 2012. Principles of Composite Material Mechanics. CRC Press, New York.
Grassi, M., Zhang, X., Meo, M., 2002. Prediction of stiffness and stresses in z-fibre reinforced composite laminates. Compos. Part A Appl. Sci. Manuf. 33, 1653–1664.
Greenwoo, J.H., Rose, P.G., 1974. Compressive behavior of kevlar-49 fibers and composites. J. Mater. Sci. 9, 1809–1814.
Havner, K.S., 1971. A discrete model for the prediction of subsequent yield surfaces in polycrystalline plasticity. Solid Struct. 7, 719–730.
Herring, C., Galt, J.K., 1952. Elastic and plastic properties of very small metal specimens. Phys. Rev. 85, 1060–1061.
Hutchinson, J.W., 1987. Crack tip shielding by microcracking in brittle solids. Acta Metall. 35, 1605–1619.
Hutchinson, J.W., 1989. Mechanisms of toughening in ceramics. In: Germain, P., Piau, M., Caillerie, D. (Eds.), Theoretical and Applied Mechanics. Elsevier, North-Holland.
Jones, R.M., 1999. Mechanics of Composite Materials. Taylor & Francis, New York.
Kaw, A.K., 2006. Mechanics of Composite Materials. Taylor & Francis, Boca Raton.
Lange, F.F., 1970. Interaction of a crack front with a second-phase dispersion. Philos. Mag. 22, 983–992.
Levy, A., Papazian, J.M., 1990. Tensile properties of short fiber-reinforced sic/al composites. 2. Finite-element analysis. Metall. Trans. A 21, 411–420.
Li, Z.H., Schmauder, S., Wanner, A., Dong, M., 1995. Expressions to characterize the flow behavior of particle-reinforced composites based on axisymmetrical unit-cell models. Scr. Metall. Mater. 33, 1289–1294.
Pearson, R.A., Yee, A.F., 1993. Toughening mechanisms in thermoplastic-modified epoxies. 1. Modification using poly(phenylene oxide). Polymer 34, 3658–3670.
Qin, Q.H., 1993. Nonlinear analysis of Reissner plates on an elastic foundation by the BEM. Int. J. Solids Struct. 30, 3101–3111.
Qin, Q.H., 1998. Nonlinear analysis of plate bending by BEM. In: Aliabadi, M.H. (Ed.), BEM Formulation for Plate Bending Analysis. Computational Mechanics Publications, Southampton, pp. 249–274.
Qin, Q.H., 2000. The Trefftz Finite and Boundary Element Method. WIT Press, Southampton.
Qin, Q.H., 2004a. Material properties of piezoelectric composites by BEM and homogenization method. Compos. Struct. 66, 295–299.
Qin, Q.H., 2004b. Micromechanics-BE solution for properties of piezoelectric materials with defects. Eng. Anal. Boundary Elem. 28, 809–814.
Qin, Q.H., 2005. Micromechanics-BEM analysis for piezoelectric composites. Tsinghua Sci. Technol. 10, 30–34.
Qin, Q.H., 2009. Boundary element method. In: Yang, J.S. (Ed.), Special Topics in the Theory of Piezoelectricity. Springer, Cambridge, MA, pp. 137–168.

Qin, Q.H., Huang, Y.Y., 1990. BEM of postbuckling analysis of thin plates. Appl. Math. Model. 14, 544–548.
Qin, Q.H., Swain, M.V., 2004. A micro-mechanics model of dentin mechanical properties. Biomaterials 25, 5081–5090.
Qin, Q.H., Yang, Q.S., 2008. Macro-micro Theory on Multifield Coupling Behaivor of Heter-eogenous Materials. Higher Education Press and Springer, Beijing.
Qin, Q.H., Yu, S.W., 1997. Using Mori-Tanaka method for effective moduli of cracked thermopiezoelectric materials. In: ICF 9-Sydney, Australia-1997, pp. 2211–2218.
Qin, Q.H., Yu, S.W., 1998. Effective moduli of piezoelectric material with microcavities. Int. J. Solids Struct. 35, 5085–5095.
Qin, Q.H., Mai, Y.W., Yu, S.W., 1998. Effective moduli for thermopiezoelectric materials with microcracks. Int. J. Fract. 91, 359–371.
Tjong, S.C., Meng, Y.Z., 1999. Microstructural and mechanical characteristics of compatibilized polypropylene hybrid composites containing potassium titanate whisker and liquid crystalline copolyester. Polymer 40, 7275–7283.
Tvergaard, V., 1990. Analysis of tensile properties for a whisker-reinforced metal matrix composite. Acta Metall. Mater. 38, 185–194.
Wang, Y., Qin, Q.H., 2007. A generalized self consistent model for effective elastic moduli of human dentine. Compos. Sci. Technol. 67, 1553–1560.
Wang, Y., Qin, Q.H., 2011. Micromechanics for determining effective material properties of dentine composites. In: Qin, Q.H., Sun, B. (Eds.), Advances in Engineering Mechanics. Nova Science Publishers, New York, pp. 319–358.
Xia, Z.H., Zhang, Y.F., Ellyin, F., 2003. A unified periodical boundary conditions for representative volume elements of composites and applications. Int. J. Solids Struct. 40, 1907–1921.
Xu, L.M., Li, C., Fan, H., Wang, B., 2008. Elastic property prediction by finite element analysis with random distribution of materials for tungsten/silver composite. J. Mater. Sci. 43, 5804–5808.
Yang, Q.S., Qin, Q.H., 2001. Fiber interactions and effective elasto-plastic properties of short-fiber composites. Compos. Struct. 54, 523–528.
Yang, Q.S., Qin, Q.H., 2003. Modelling the effective elasto-plastic properties of unidirectional composites reinforced by fibre bundles under transverse tension and shear loading. Mater. Sci. Eng. A 344, 140–145.
Yang, Q.S., Qin, Q.H., 2004. Micro-mechanical analysis of composite materials by BEM. Eng. Anal. Boundary Elem. 28, 919–926.
Ye, J., 2003. Laminated Composite Plates and Shells: 3D Modelling. Springer, London.
Yu, S.W., Qin, Q.H., 1996. Damage analysis of thermopiezoelectric properties: part II. Effective crack model. Theor. Appl. Fract. Mech. 25, 279–288.
Zahl, D.B., McMeeking, R.M., 1991. The influence of residual-stress on the yielding of metal matrix composites. Acta Metall. Mater. 39, 1117–1122.